From a discrete to a continuous model for inter-pulse interference with a frequency comb laser

M. G. Zeitouny,* M. Cui, N. Bhattacharya, and H.P. Urbach

Technische Universiteit Delft, Lorentzweg 1, 2628 CJ Delft, The Netherlands

S.A. van den Berg

VSL, Thijsseweg 11, 2629 JA Delft, The Netherlands

A. J. E. M. Janssen

Technical University Eindhoven, Department EE and EURANDOM,

LG-1, P. O. Box 513, 5600 MB Eindhoven, The Netherlands

(Dated: April 1, 2010)

Abstract

We have investigated correlation patterns generated by a frequency comb laser in a dispersive unbalanced Michelson interferometer and apply the developed formalism to the case of distance metrology. Due to group velocity dispersion, the position of the brightest fringe of the correlation pattern, which is used for distance determination, cannot be derived by simply using the definition of group refractive index of the dispersive medium. It is shown that the discrete spectrum of the optical frequency comb gives rise to correlation functions which can be represented by a series, namely a discrete correlation series. We have developed a general formalism, valid for any pulse train, extending the discrete model to a continuous model of cross-correlation functions using the Poisson summation. Our model is relevant for any offset and repetition frequency of the frequency comb. From the continuous cross-correlation model we show that, even for a homogeneous dispersive medium the position of the brightest fringe varies non-linearly for small delay distances and stabilizes for longer ones. We have compared the theoretical results to measurements of pulse propagation in air for path-lengths up to 200 m.

PACS numbers: 42.25.Hz, 42.25.Kb, 42.62.Eh

*M.Zeitouny@tudelft.nl

I. INTRODUCTION

Recent advances in the field of femtosecond pulses has led to the development of reliable sources of carrier-envelope-phase stabilized femtosecond pulses [1–3]. The pulse train generated by such a source has a frequency spectrum that consists of discrete, regularly spaced lines known as an optical frequency comb. In this case both the frequency repetition and the carrier-envelope-offset (CEO) frequency, are referenced to a frequency standard, like an atomic clock. As a result the accuracy of the frequency standard is transferred to the optical domain, with the frequency comb as transfer oscillator. These unique properties allow the frequency comb to be applied as a versatile tool, not only for time and frequency metrology [4–7], but also in fundamental physics [8, 9], high-precision spectroscopy [10–12] and laser noise characterization [13–15]. Moreover, the pulse-to-pulse phase relationship of the light emitted by the frequency comb has opened up a new avenue for long range highly accurate distance measurement [16–23]. Here the spatial and temporal coherence between the pulses is utilized. For non-dispersive media an arbitrary plane wave pulse would propagate unaltered in shape at the phase velocity of the wave field in the medium. In that case, the analysis of the resulting interfering field or correlation patterns is straightforward. However, the analysis acquires complexity for pulse propagation in a dispersive medium like air [21, 22].

Propagation of individual pulses in dispersive media has been extensively studied over the last decades. Most analysis of ultrashort pulses for propagation [24–26] or interference [27] is based on Gaussian pulse models. Under this assumption, the theory of dispersive pulse propagation has been developed, considering phase velocity, group velocity and the group delay dispersion. The electric fields of the Gaussian pulses will generate symmetric interference patterns even if second-order dispersion is taken into account. However, practical applications like distance measurement use laser pulses with asymmetric non-Gaussian spectra and therefore require a generalized approach.

In this paper, we present a study of the formation of correlation patterns in a dispersive unbalanced Michelson interferometer using a frequency comb laser as a source. This study is specifically intended for distance measurement in dispersive media. For accurate distance determination, precise knowledge of the position of the brightest fringe, the fringe having maximum contrast, of the correlation pattern is required. We show the influence of the

propagation of pulses in air on the position of the brightest fringe of the correlation pattern for non-symmetric spectra. The position of maximum coherence is linked to the asymmetry of the spectrum and the environmental parameters. Theoretical and numerical analysis show the difference between the correlation patterns generated by symmetric spectra (such as a Gaussian spectrum) and arbitrary spectra emitted from a laser.

We approach the problem by representing the correlation function from the optical frequency comb by a discrete correlation series. Using the Poisson summation formula we extend the above formalism to a continuous model of cross-correlation functions. Our model is relevant for any offset and repetition frequency of the frequency comb. The model allows us to show that even for a homogenous dispersive medium the position of the brightest fringe varies non-linearly for small delay distances and stabilizes for longer ones. The distance where non-linear effects are important is shown to be dependent on the properties of the dispersive media and the initial spectrum of the transmitted pulse. In case of very large delay distances the particular values of the frequencies present in the spectrum play an important role since only specific frequencies contribute to specific fringes in the cross-correlation. Therefore, the precise values of the offset and repetition frequencies become important and the model can be used to determine the properties of the cross-correlations in the asymptotic limit of large delay distances, as compared to a model where the offset frequency is ignored. This makes the present continuous model valid for a large range of delay distances. The properties of the cross-correlation functions at large delays are studied using asymptotic analysis in another paper [28].

The pulse-to-pulse phase stability of the frequency comb source offers the opportunity, for the first time, to give a comparison between a theoretical and experimental analysis of the formation of temporal interference fringes in dispersive media. The theory and numerical simulation developed in this paper will be compared to measurements of path lengths up to 200 m.

This paper is organised as follows. In Section II, a theoretical model of the cross-correlation functions obtained from the discrete spectrum of the frequency comb has been developed followed by a comparison with some experimental measurements. In Section III, we extend the discrete formulation of the cross-correlation to a continuous model using the Poisson summation formula. This is followed in Section IV by a study of the position of the brightest fringe in the cross-correlation based on the continuous model and the quadratic

phase approximation. In Section V we estimate the distance where non-linear effects are dominant in a dispersive medium. Finally, the main conclusions of this work are summarised in Section VI.

II. ANALYSIS OF PULSE CROSS-CORRELATION FUNCTIONS

First, we give a short description of a generalized distance metrology setup using a Michelson interferometer. In 2004, a scheme for measuring long distances in space with a stabilized

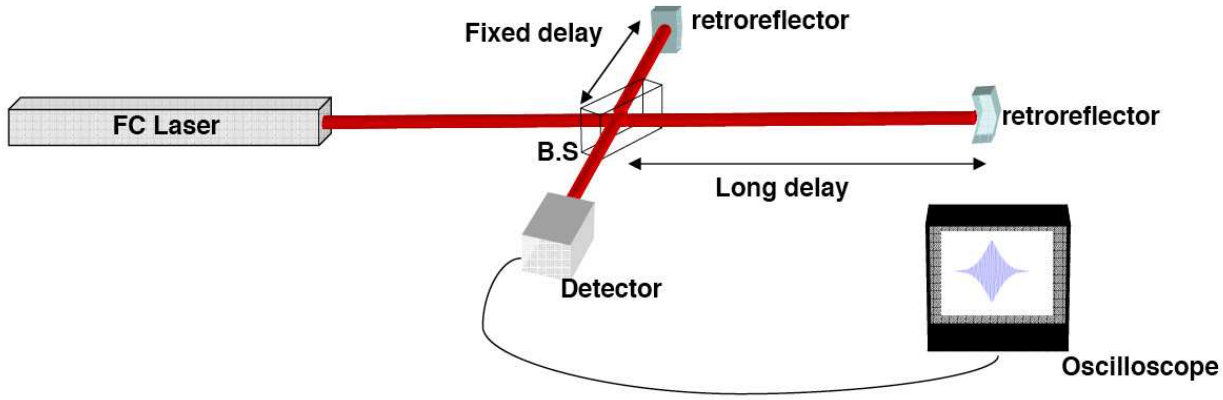

FIG. 1. Schematic of the experimental setup.

femtosecond frequency comb was proposed [16]. The scheme is based on a Michelson type interferometry with optical interference between individual pulses. The basic elements of this scheme are shown in Fig. 1. The pulse train from the laser is split into two beams which are recombined after having passed through various optical delays. The short arm is scanned over a fixed range using, among others, a piezoelectric-transducer, while the long arm is displaced over a distance that is to be determined. The intensity of the recombined beam is recorded as a function of the variable delay, i.e. piezo-element positions. In vacuum, a maximum coherence is obtained when the path length difference $q \times l_{pp}$ between both arms is equal to an integer q multiple of the effective laser cavity length in vacuum $l_{pp} = c/f_r$ or the pulse-to-pulse distance, where f_r is the pulse repetition of the laser and c is the velocity of light in vacuum. In dispersive media, one may expect that $l_{pp} = c/(n_g \times f_r)$ where n_g denotes the group refractive index of the medium. The group refractive index n_g and/or the corresponding group velocity of a pulse propagating in dispersive media has been the

subject of extensive analysis [24–26, 29]. Group velocity has been traditionally described as the rate at which the envelope of a group of waves travels through the dispersive medium. Propagation in a dispersive medium, however, leads to substantial broadening and shape deformation, referred to as chirp in the sequel, of the pulse due to group velocity dispersion [24]. For the case of an ultrashort pulse in a dispersive medium the classical definition of group velocity becomes questionable, in particular in the region of anomalous dispersion [25]. However, even in the case of quadratic dispersive media in the region of normal dispersion with negligible absorption, the use of group velocity for metrological purposes can be misleading, this is the focus of the present study. For the case of distance measurement, the pulse traveling in the long arm acquires a chirp which modifies the shape and width of correlation patterns extensively. The position of the maximum of the correlation differs considerably from $q \times l_{pp}$ where l_{pp} is calculated using the group refractive index n_g at the maximum of the source spectrum. The relation between the position of the maximum of a correlation pattern and this particular choice of n_g will be discussed rigourously in the next section.

The complete mathematical and physical basis for the group velocity approximation in the context of a pulse propagating through quadratic dispersive media was laid by Jones [29] using the quasimonochromatic or slowly-varying envelope approximation. An alternative treatment using ABCD matrices was given by Dijaili *et al.*[26]. We extend the treatment of pulse propagation to the interference pattern formed by the overlap of the chirped pulse with a non-chirped one. Our treatment is mainly for pulses with a non-symmetric spectrum propagating in a passive dispersive media like air in the regime of normal dispersion.

A. Cross-correlations in dispersive media

The field cross-correlation is readily measured experimentally by placing a slow detector at the output of the Michelson interferometer. The detector is illuminated by the input electric field $\mathcal{E}(x_1, t)$ coming from one arm, and by the delayed field $\mathcal{E}(x_2, t)$ from the other arm. If the time response of the detector is much larger than the time duration of the signal $\mathcal{E}(t)$, or if the recorded signal is integrated, the detector measures the intensity. In this section we calculate the intensity detected by a slow detector as the interference of two electric fields which have traveled the distances x_1 and x_2, respectively.

The frequency spectrum emitted by a mode-locked laser consists of a comb of regularly spaced frequencies

$$\omega_m = m\omega_r + \omega_0, \tag{1}$$

where ω_0 is the common offset frequency, m is an positive integer and ω_r is the repetition frequency f_r expressed in angular notation

$$\omega_r = 2\pi f_r = \frac{2\pi}{T_r} \ , \ T_r = \frac{1}{f_r}. \tag{2}$$

Here T_r is the time distance between the pulses. The offset frequency ω_0 is caused by the difference between the group velocity and the phase velocity inside the laser cavity. Both ω_0 and ω_r are stabilised to an atomic clock.

In our experiments we use a Ti:sapphire laser. The central frequency of the comb is $\omega_c = 2.3254 \times 10^{15}$ Hz, corresponding to a wavelength of 810 nm in vacuum, the bandwidth is typically $\Delta\omega \approx 5 \times 10^{14}$ Hz, which corresponds to a pulse width of $\Delta x \approx 12$ μm and a pulse duration of 40 fs. The frequency offset is $\omega_0 \approx 2\pi \times 180 \times 10^6$ rad/s and the repetition frequency is $\omega_r = 6.28 \times 10^9$ rad/s, corresponding to a cavity length $l_{pp} = 30$ cm and period $T_r \approx 1$ns.

We now aim to obtain an expression for the cross-correlation function from the laser source described above in presence of dispersive media. We use the Fourier transform as

$$(\mathcal{F}f)(\omega) = \int_{-\infty}^{\infty} f(t) \exp(-i\omega t) dt \tag{3}$$

with the inversion formula

$$f(t) = \frac{1}{2\pi} \int_{-\infty}^{\infty} (\mathcal{F}f)(\omega) \exp(i\omega t) d\omega, \tag{4}$$

and Parseval's formula

$$\int_{-\infty}^{\infty} (\mathcal{F}f)(\omega)(\mathcal{F}g)^*(\omega) d\omega = 2\pi \int_{-\infty}^{\infty} f(t) g^*(t) dt \tag{5}$$

The field of the pulse emitted by the laser, propagating in the direction of positive x, at $x = 0$ can be written as

$$\mathcal{E}(0,t) = \sum_{m=0}^{\infty} A_m \cos[(m\omega_r + \omega_0)t + \phi_m] \tag{6}$$

where A_m is a real amplitude and ϕ_m is the phase. In the calculations that follow it will be convenient to use negative frequencies.

We write Eq. (6) as

$$\begin{aligned}\mathcal{E}(0,t) &= \mathrm{Re}\sum_{m=0}^{\infty} A_m \exp(i\phi_m)\exp[i(m\omega_r+\omega_0)t] \\ &= \mathrm{Re}\left[\exp(i\omega_0 t)\mathcal{E}^p(0,t)\right] \end{aligned} \tag{7}$$

with

$$\mathcal{E}^p(0,t) = \sum_{m=0}^{\infty} a_m \exp(im\omega_r t) \tag{8}$$

where $a_m = A_m \exp(i\phi_m)$. We have

$$\begin{aligned}\mathcal{F}\left[\mathcal{E}^p(0,.)\right](\omega) &= \int_{-\infty}^{\infty} \mathcal{E}^p(0,t)\exp(-i\omega t)dt \\ &= \sum_{m=0}^{\infty} a_m \int_{-\infty}^{\infty} \exp[i(m\omega_r-\omega)t]dt \\ &= 2\pi\sum_{m=0}^{\infty} a_m \delta(\omega - m\omega_r) \end{aligned} \tag{9}$$

where the dot in the left-hand side is used to indicate the variable (in this case, the Fourier transform is taken with respect to time 't'). It follows from Eq. (9) that the Fourier transform of the pulse emitted by the laser is

$$\begin{aligned}\mathcal{F}\left[\mathcal{E}(0,.)\right](\omega) &= \frac{1}{2}\mathcal{F}\left[\exp(i\omega_0 t)\mathcal{E}^p(0,.)\right](\omega) + \frac{1}{2}\mathcal{F}\left[\exp(-i\omega_0 t)\mathcal{E}^p(0,.)^*\right](\omega) \\ &= \pi\sum_{m=0}^{\infty} a_m \delta(\omega - m\omega_r - \omega_0) + \pi\sum_{m=0}^{\infty} a_m^* \delta(\omega + m\omega_r + \omega_0) \end{aligned} \tag{10}$$

Next we consider the propagation of the pulse in a dispersive medium with refractive index $n(\omega)$ and assuming that the pulse propagates in the direction of positive x we can write the initial field at position $x = 0$ and time t as

$$\mathcal{E}(0,t) = \frac{1}{2\pi}\int_{\infty}^{\infty} \mathcal{F}\left[\mathcal{E}(0,.)\right](\omega)\exp(i\omega t)d\omega. \tag{11}$$

From this we get the field at x

$$\begin{aligned}\mathcal{E}(x,t) &= \frac{1}{2\pi}\int_{-\infty}^{\infty} \mathcal{F}\left[\mathcal{E}(0,.)\right](\omega)\exp\left[i\omega(t - n(\omega)\frac{x}{c})\right]d\omega \\ &= \frac{1}{2\pi}\int_{-\infty}^{\infty} \mathcal{F}\left[\mathcal{E}(x,.)\right](\omega)\exp(i\omega t)d\omega. \end{aligned} \tag{12}$$

In addition, we assume that the medium is lossless, i.e. that $n(\omega)$ is real for all frequencies of the comb.

The Fourier transform of the field with respect to time is

$$\mathcal{F}\left[\mathcal{E}(x,.)\right](\omega) = \pi \sum_{m=0}^{\infty} a_m \exp\left[-i(m\omega_r+\omega_0)n(m\omega_r+\omega_0)\frac{x}{c}\right]\delta(\omega - m\omega_r - \omega_0)$$
$$+\pi \sum_{m=0}^{\infty} a_m^* \exp\left[i(m\omega_r+\omega_0)n(m\omega_r+\omega_0)\frac{x}{c}\right]\delta(\omega + m\omega_r + \omega_0) \quad (13)$$

where we used

$$n(-\omega) = n(\omega) \quad (14)$$

Consider now the interference of fields that have propagated over the distances x_1 and x_2, respectively. The total field at a given time is then:

$$\mathcal{E}_{tot}(x_1, x_2, t) = \mathcal{E}(x_1, t) + \mathcal{E}(x_2, t). \quad (15)$$

A detector is used with a broad detection window

$$-\frac{T_d}{2} < t < \frac{T_d}{2} \quad (16)$$

with $T_d \approx 1\text{ms} \cong 10^6 T_r$. We define

$$\chi_{T_d}(t) = \begin{cases} \frac{1}{T_d} & \text{if } -\frac{T_d}{2} < t < \frac{T_d}{2}, \\ 0 & \text{otherwise.} \end{cases} \quad (17)$$

The Fourier transform of Eq. (17) is given by

$$\mathcal{F}\left[\chi_{T_d}\right](\omega) = \frac{\sin\left(\omega\frac{T_d}{2}\right)}{\omega\frac{T_d}{2}} = \text{sinc}\left(\frac{1}{2}\omega T_d\right) \quad (18)$$

The signal measured by the 'slow' detector is

$$\begin{aligned} P(x_1, x_2) &= \frac{1}{T_d}\int_{-T_d/2}^{T_d/2} \left|\mathcal{E}_{tot}(x_1, x_2, t)\right|^2 dt \\ &= \frac{1}{T_d}\int_{-T_d/2}^{T_d/2} \left|\mathcal{E}(x_1, t)\right|^2 dt + \int_{-T_d/2}^{T_d/2} \left|\mathcal{E}(x_2, t)\right|^2 dt \\ &\quad + \frac{2}{T_d}\text{Re}\int_{-T_d/2}^{T_d/2} \mathcal{E}(x_1, t)\mathcal{E}(x_2, t)^* dt \end{aligned} \quad (19)$$

For $i, j = 1, 2$ we consider the integral

$$\begin{aligned} \Gamma(x_i, x_j) &= \frac{1}{T_d}\text{Re}\int_{-T_d/2}^{T_d/2} \mathcal{E}(x_i, t)\mathcal{E}(x_j, t)^* dt \\ &= T_d\text{Re}\int_{-\infty}^{\infty} \chi_{T_d}(t)\mathcal{E}(x_i, t)\chi_{T_d}(t)\mathcal{E}(x_j, t)^* dt \\ &= \frac{T_d}{2\pi}\text{Re}\int_{-\infty}^{\infty} \mathcal{F}\left[\chi_{T_d}(.)\mathcal{E}(x_i, .)\right](\omega)\,\mathcal{F}\left[\chi_{T_d}(.)\mathcal{E}(x_j, .)\right]^*(\omega) d\omega \end{aligned} \quad (20)$$

where in the last step we used the Parseval's theorem. Next we write

$$\begin{aligned}\mathcal{F}\left[\chi_{T_d}(.)\mathcal{E}(x_i,.)\right](\omega) &= \frac{1}{2\pi}\mathcal{F}\left[\chi_{T_d}\right](\omega) * \mathcal{F}\left[\mathcal{E}(x_i,.)\right](\omega) \\ &= \frac{1}{2}\sum_{m=0}^{\infty} a_m \exp\left[-i(m\omega_r+\omega_0)n(m\omega_r+\omega_0)\frac{x_i}{c}\right]\mathrm{sinc}\left[(\omega-m\omega_r-\omega_0)\frac{T_d}{2}\right] \\ &+ \frac{1}{2}\sum_{m=0}^{\infty} a_m^* \exp\left[i(m\omega_r+\omega_0)n(m\omega_r+\omega_0)\frac{x_i}{c}\right]\mathrm{sinc}\left[(\omega+m\omega_r+\omega_0)\frac{T_d}{2}\right]\end{aligned} \tag{21}$$

Since $T_d \gg T_r = 2\pi/\omega_r$, the product of two functions $\mathcal{F}\left[\chi_{T_d}\right](\omega \pm m\omega_r \pm \omega_0)$ with different m's is negligible. Therefore, by using Eq. (21), Eq. (20) can be written as

$$\begin{aligned}\Gamma(x_i,x_j) &\approx \frac{T_d}{2\pi}\sum_{m=0}^{\infty}\frac{1}{2}|a_m|^2 \exp\left[-i(m\omega_r+\omega_0)n(m\omega_r+\omega_0)\frac{(x_i-x_j)}{c}\right] \\ &\qquad \times \int_{-\infty}^{\infty}\left[\mathrm{sinc}\left[(\omega-m\omega_r-\omega_0)\frac{T_d}{2}\right]\right]^2 d\omega \\ &+ \frac{T_d}{2\pi}\sum_{m=0}^{\infty}\frac{1}{2}|a_m|^2 \exp\left[i(m\omega_r+\omega_0)n(m\omega_r+\omega_0)\frac{(x_i-x_j)}{c}\right] \\ &\qquad \times \int_{-\infty}^{\infty}\left[\mathrm{sinc}\left[(\omega+m\omega_r+\omega_0)\frac{T_d}{2}\right]\right]^2 d\omega \\ &= \frac{T_d}{2\pi}\sum_{m=0}^{\infty}|a_m|^2\cos\left[(m\omega_r+\omega_0)n(m\omega_r+\omega_0)\frac{(x_i-x_j)}{c}\right]\int_{-\infty}^{\infty}\left[\mathrm{sinc}\left(\omega\frac{T_d}{2}\right)\right]^2 d\omega \\ &= \sum_{m=0}^{\infty}|a_m|^2\cos\left[(m\omega_r+\omega_0)n(m\omega_r+\omega_0)\frac{(x_i-x_j)}{c}\right]\end{aligned} \tag{22}$$

Here it has been used that $\int_{-\infty}^{\infty}\left[\mathrm{sinc}\left(\omega\frac{T_d}{2}\right)\right]^2 d\omega = 2\pi/T_d$. Since the measured intensity will not depend explicitly on x_1 and x_2 we can take $X = x_1 - x_2$ and write

$$\Gamma(X) \equiv \Gamma(x_i,x_j) \tag{23}$$

Then

$$P(x_1,x_2) = 2\Gamma(0) + 2\Gamma(X) \tag{24}$$

and the cross-correlation is, apart from the DC-background $2\Gamma(0)$ and a factor of 2, given by

$$\Gamma(X) = \sum_{m=0}^{\infty}|a_m|^2\,\cos\left[(m\omega_r+\omega_0)n(m\omega_r+\omega_0)\frac{X}{c}\right] \tag{25}$$

where $|a_m|^2 \equiv$ Power Spectral Density (PSD). This shows that the first-order cross-correlation function requires the knowledge of the source spectrum and not the pulse electric

field. Numerical analysis based on Eq. (25) with comparison to measured data will be given in the next part of this section.

B. Measured cross-correlations compared with numerical model

In the present section we will compare numerically simulated cross-correlations using the results from the previous section with our measured data.

A general description of the experimental arrangement was given in the introduction of the section II. The detailed measurement setup is described in [22]. The aim of this experiment was to demonstrate absolute distance metrology using a frequency comb laser as a source in an unbalanced Michelson interferometer setup.

As mentioned earlier, analysis of the cross-correlation patterns to extract the distance requires an accurate knowledge of the position of the brightest fringe of the correlation pattern. The pulse propagating in the long arm of the interferometer acquires considerable chirp due to the dispersion in air leading to changes in shape and width of the resulting cross-correlation patterns. The asymmetry of the spectral profile of the pulses also plays a role in this. The spectrum of the laser source has been obtained from two separate measurements. First, a direct measurement using an Ocean Optics spectrometer was done. The spectrum was also retrieved from the measured first order auto-correlation pattern (Fourier transform spectroscopy). We found good agreement between both the measured spectra, as shown in Fig. 2.

The spectral content of the initial pulse is the main input for the numerical model. Using the corrected updated Edlén's equation[30] for the refractive index of air, 8×10^4 spectral lines fitted to the profile of the spectrum of the laser are propagated. Specific details of the laser, the spectra and the pulse were mentioned in the previous section. Cross-correlation patterns are calculated for different pulse propagation distances which are an integer multiple of the distance between two successive pulses. The frequency comb laser emits broadband pulses which, after traveling through different paths in the interferometer, superpose and form interference fringes. For distance measurements, the brightest fringe position is used in data analysis since a maximum fringe intensity indicates the occurrence of a maximum temporal coherence between superposed pulses. In vacuum, a maximum coherence indicates

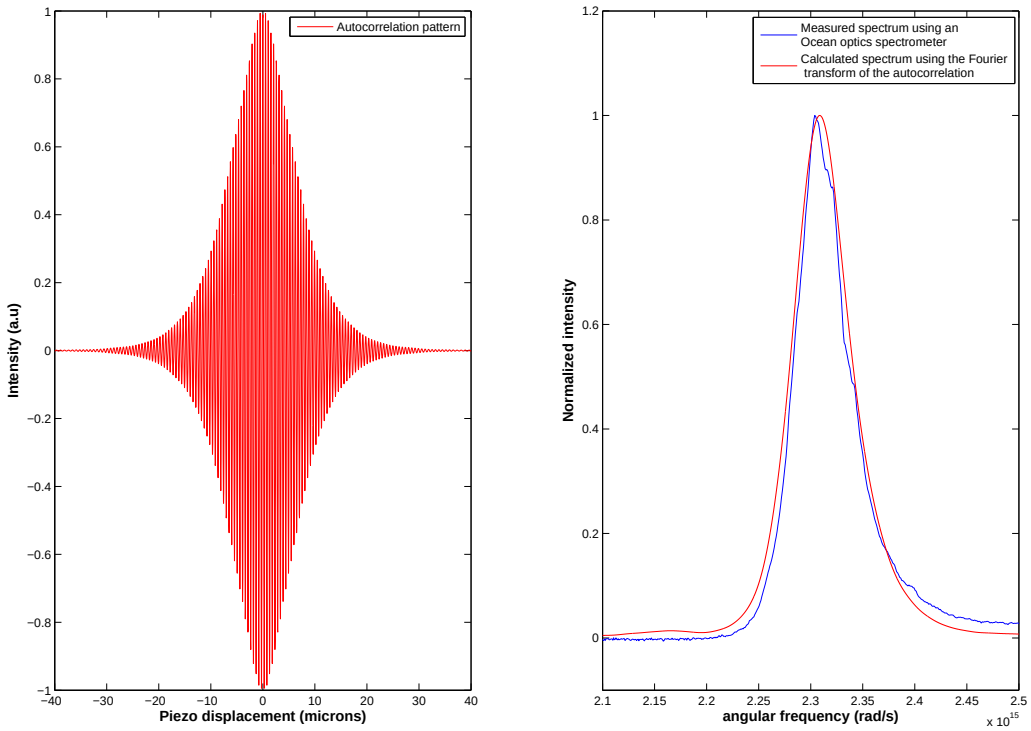

FIG. 2. **Left:** Autocorrelation pattern. **right:** Laser spectra directly measured compared with one retrieved from the autocorrelation

that the path length difference in the Michelson interferometer is exactly $q \times l_{pp}$ where $l_{pp} = 2\pi c/\omega_r$ and q is an integer. Carrying out distance measurements in air requires a detailed knowledge of the dispersion relation. The phase delay is

$$v_p(\omega) = \omega/k(\omega) = c/n(\omega) \tag{26}$$

where $k(\omega)$ is the wavenumber and $n(\omega)$ is the refractive index given by the Edlén's equation. After a certain propagation length, the delay of the pulse envelope, the group delay, is equal to $v_g = d\omega/dk(\omega) = c/n_g$. Here n_g is the group refractive index defined at the carrier frequency of the pulse (ω_c), conventionally accepted as the frequency with the maximum intensity in the spectrum, and given by

$$n_g = n(\omega_c) + \omega_c \left[\frac{d(n(\omega))}{d\omega}\right]_{\omega_c} \tag{27}$$

For interferometric distance metrology, the maximum fringe visibility is reached at a given delay L. In vacuum $L = q \times l_{pp}$ and in a dispersive medium $L_n = q \times l_{pp}/n_g$. We would

like to emphasize here that the position of L_n does not coincide with the position of the maximum of the cross-correlation pattern. The formation of a cross-correlation after pulse propagates in dispersive media does not depend only on the individual pulse path in one arm, but rather on the interference between pulses which have encountered different delays. The two positions coincide only when the medium is linearly dispersive.

Simulated (Eq. 25) and corresponding measured cross-correlation patterns are shown in Fig. 3. The simulated and measured cross-correlation patterns correspond to path length differences of 20, 40, 60, 80, and 100 m in air. In general, the shapes show good agreement.

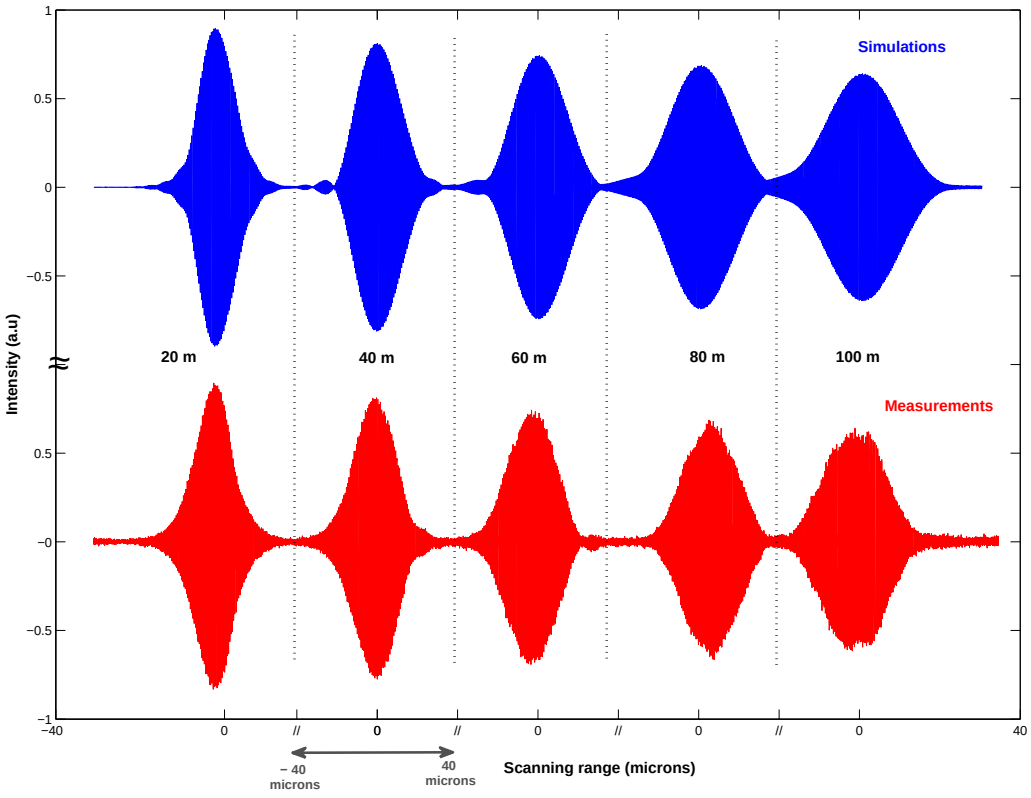

FIG. 3. Measured patterns compared with simulation of various cross-correlation in air under the same environmental conditions.

Simulated and measured patterns both show similar chirp and broadening. It can be seen that the numerical model can account for the effect of non-linear dispersion on the pulses which have an asymmetric frequency spectrum. Full width at $1/e$ of the maximum ($FW_{1/e}$) of measured and simulated correlation patterns are given in Fig. 4. The comparison is done for 0 up to 200 m propagation in air . For short distances (less than 80 m), $FW_{1/e}$ of

both simulated and measured pattern agree very well. After 80 m of path length difference, a disagreement is observed. This difference is mostly due to the unpredictable effects of vibrations in the interferometer and air turbulence in the measurement room. A comparison

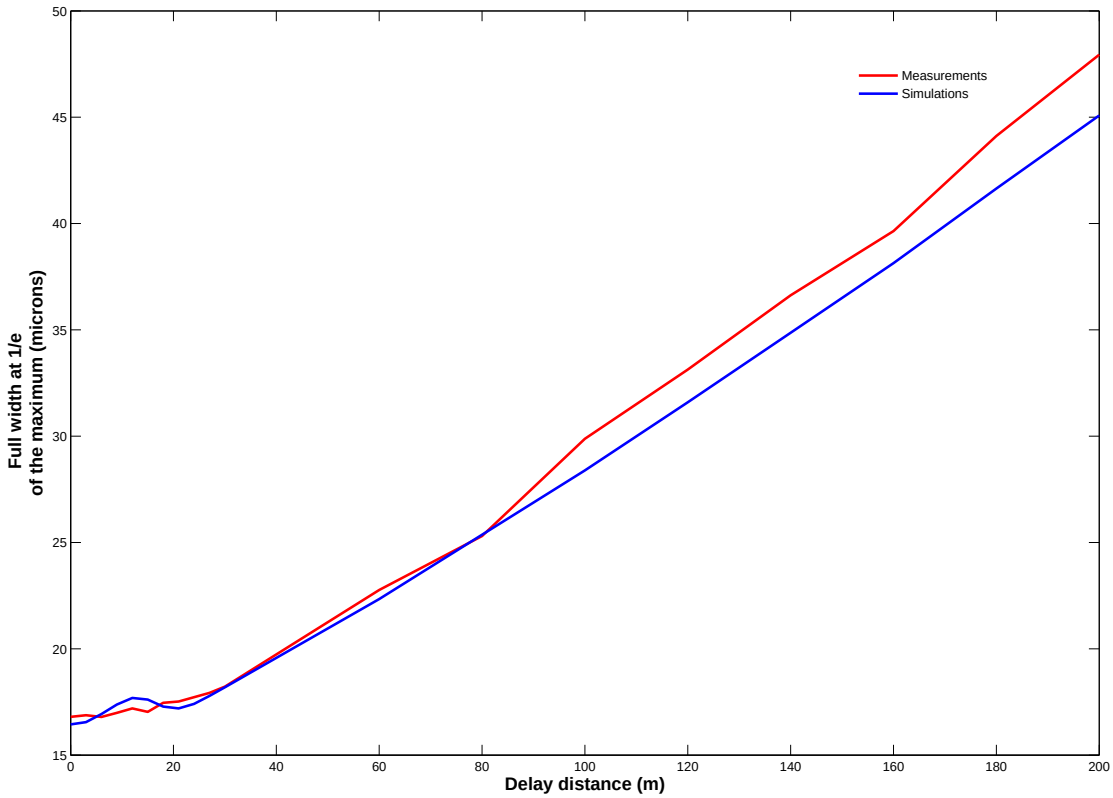

FIG. 4. Comparison of the broadening of cross-correlation patterns between simulated and measured data

between the numerical and experimental correlations for two large delay distances (160 and 200 m) is presented in Fig. 5 . Fig. 5.c and Fig. 5.f clearly show that measured patterns suffer from an extra broadening compared to the simulated ones. Furthermore we observe that the chirp has stabilized and the correlations show only a linear broadening. To demonstrate this effect, let us consider R_{HW} and L_{HW} be the right and the left half width at $1/e$ of the maximum respectively (see Fig.5.a). We define the chirp ratio as follows

$$\text{chirp ratio} = \frac{R_{HW}}{L_{HW}} \tag{28}$$

Results for Eq. 28 from the measured and simulated patterns are shown in Fig. 6 for propagation from 0 to 200 m in air. From our simulations we note that the chirp reaches its

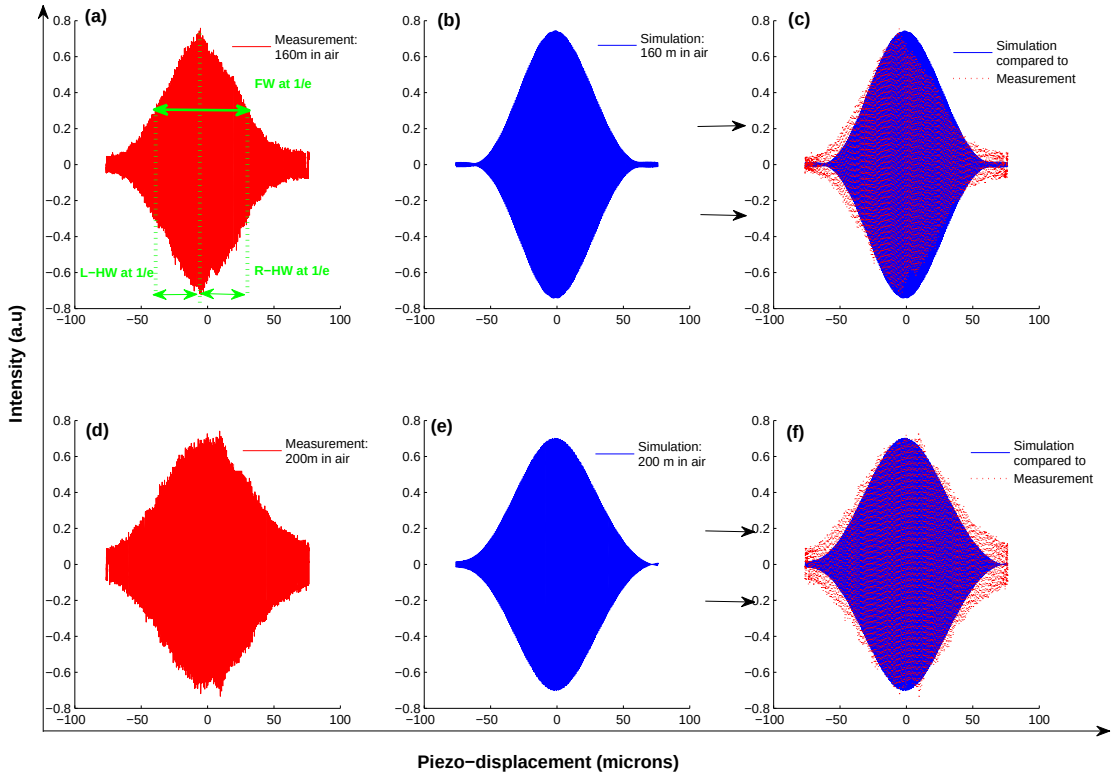

FIG. 5. Comparison between measured and simulated cross-correlation patterns for 160 m and 200 m in air to evaluate shape distortion arising from asymmetric spectra.

maximum at a distance of ~ 30 m. After 30 m, this ratio decays and tends asymptotically to a constant value for large delays (> 150 m). These numerical and experimental observations will be rigorously investigated in the next section.

C. Numerical study of the correlation patterns as a function of power spectral density

From Eq. (25) we note that the formation of the cross-correlation function depends on the spectral distribution of the laser source. In this section we discuss numerically the behaviour of cross-correlation patterns using various types of Power Spectral Densities (PSD's). The numerical study will be based on spectral distributions that are symmetric (even) e.g. Gaussian compared to distributions which are not even and closer to measured

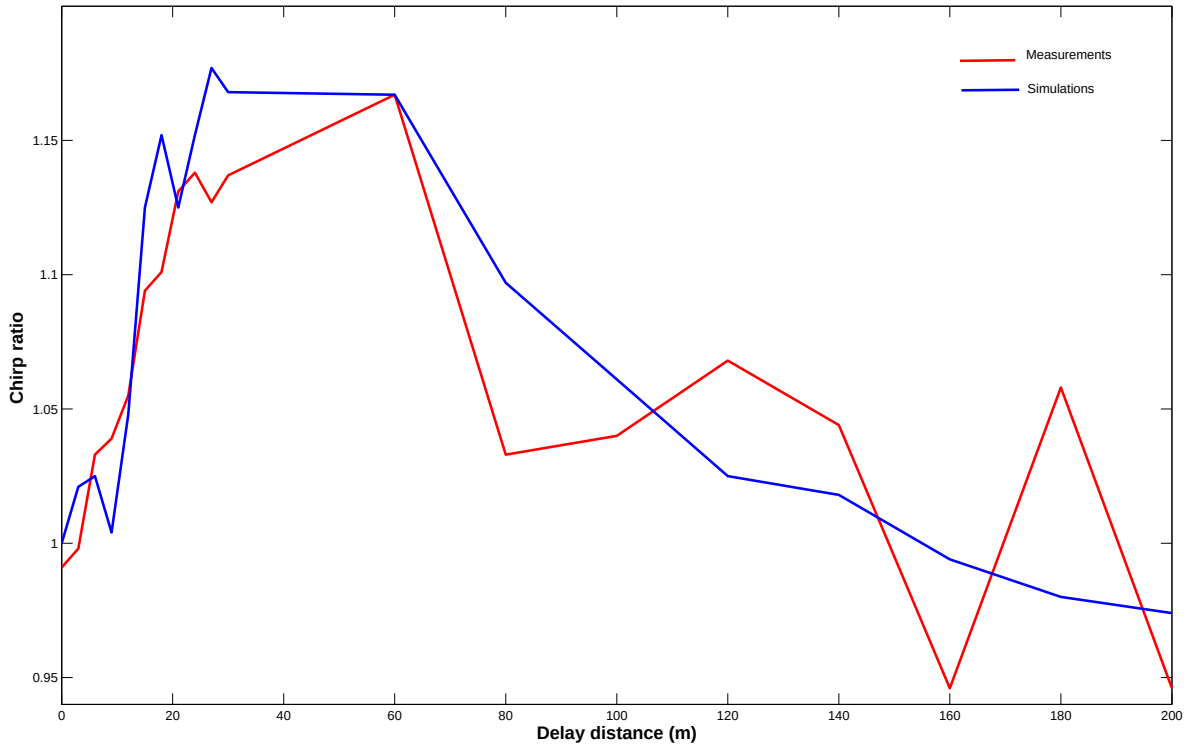

FIG. 6. Analysis of shape distortion of measured and simulated cross-correlation patterns.

spectrum.

Figure 7 illustrates the cross-correlation patterns generated by various types PSD's in two different media. Figure 7.a shows an experimental asymmetric power spectral density, a Sech^2 and a Gaussian PSD. Using these PSD's we have simulated the cross-correlation function in air and BK7 glass by taking two distances, one relatively short and the other relatively long. In the case where the PSD is symmetric, the cross-correlations remain symmetric without showing any shift with respect to the zero position of the scanning. Only when the PSD is asymmetric as in a general experiment, the position and the shape of the cross-correlations are affected. In both cases of symmetric and asymmetric spectra considerable broadening is observed for longer distances.

To illustrate the effects of asymmetric PSD's in non-linear dispersive media, we will take

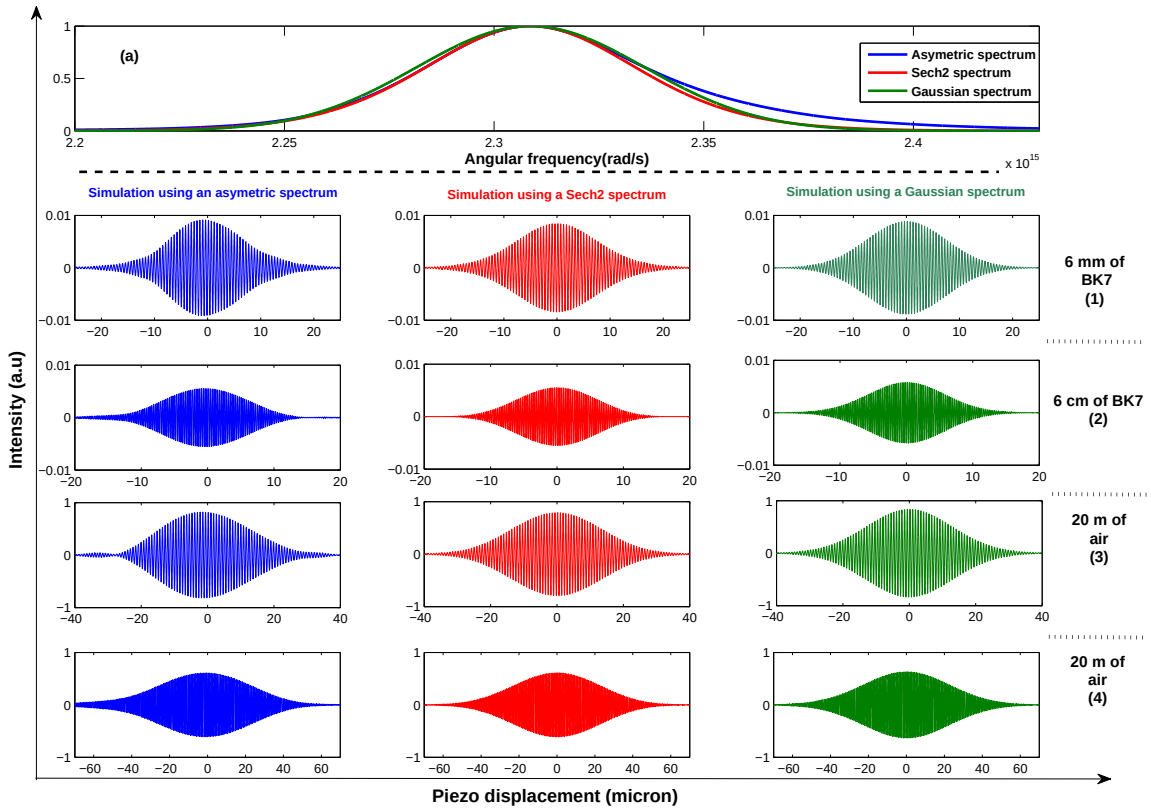

FIG. 7. Comparison between cross-correlations in different dispersive media generated using symmetric and asymmetric power spectral densities.

the following example of an asymmetric Gaussian pulse

$$a(\omega) = \begin{cases} \exp\left[-\frac{(\omega-\omega_c)^2}{2\sigma^2(1-a_r)^2}\right] & \omega \leq \omega_c, \\ \\ \exp\left[-\frac{(\omega-\omega_c)^2}{2\sigma^2(1-a_l)^2}\right] & \omega > \omega_c, \end{cases} \tag{29}$$

where a_r and a_l are the decay parameters for the regions to the right and to the left of ω_c, respectively, and ω_c is the frequency of the PSD where intensity is maximum. Two cases have been considered. First, for $a_l = 0$ and $a_r = 0.5$ the corresponding PSD with the simulated cross-correlation patterns for two different distances are shown in Fig. 8.a while for $a_r = 0$ and $a_l = 0.5$, the corresponding patterns are shown in Fig. 8.b. It is clearly seen that the behaviour of the first-order cross-correlation pattern is strongly affected by the shape of the PSD of the source. More importantly, the position of the absolute maximum of the cross-correlation is shifted.

Finally, we would like to mention the effect of the environmental parameters i.e. temper-

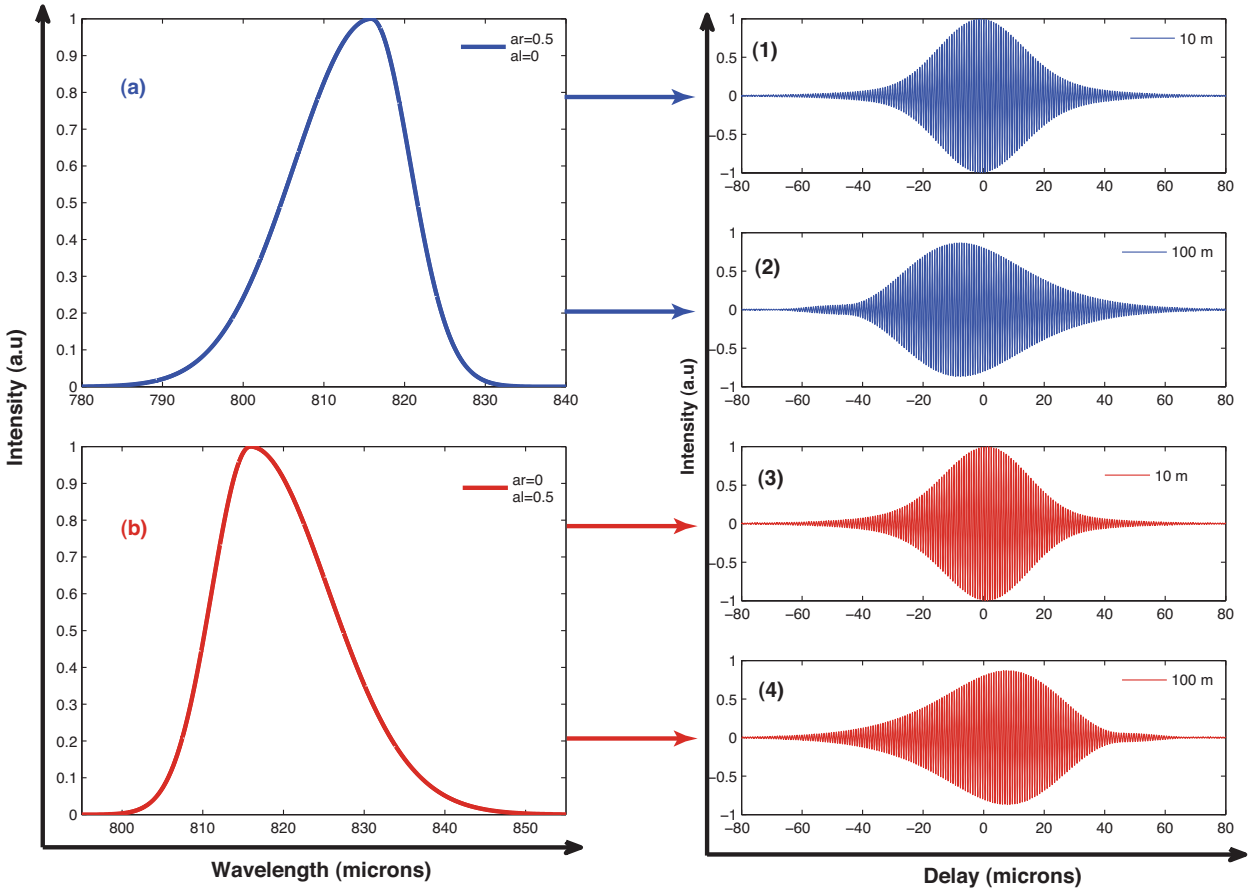

FIG. 8. (a) Right asymmetric Gaussian PSD from Eq. 29 used to compute cross-correlations for distances of 10 m and 100 m. (b) Left asymmetric Gaussian PSD from Eq. 29 used to compute cross-correlations for distances of 10 m and 100 m.

ature, pressure, and humidity of the air. Environmental fluctuation has the biggest influence on the accuracy of the measured distance. In Fig. 9, we consider the example of simulated correlation patterns at 60m pulse propagation for subtle changes in the three relevant parameters. The position of the fringe at the maximum of the correlation pattern obtained for 20°C, 1013.25 hPa and 45 % humidity is taken as a reference distance and centered at '0'. Fig. 9.a shows that for a 0.2°C temperature variation the maximum of the correlation pattern shifts by 5.36 μm from the reference. In Fig. 9.b the pressure has been increased 1hPa resulting in a 10.34 μm shift. A 1% variation in humidity shows a shift of 0.527 μm as seen in Fig. 9.c. It is known that the variation of the environmental parameters affects the correlation patterns due to the variation of the refractive index. The simulations show that the correlations patterns only shift without any extra linear broadening or chirp.

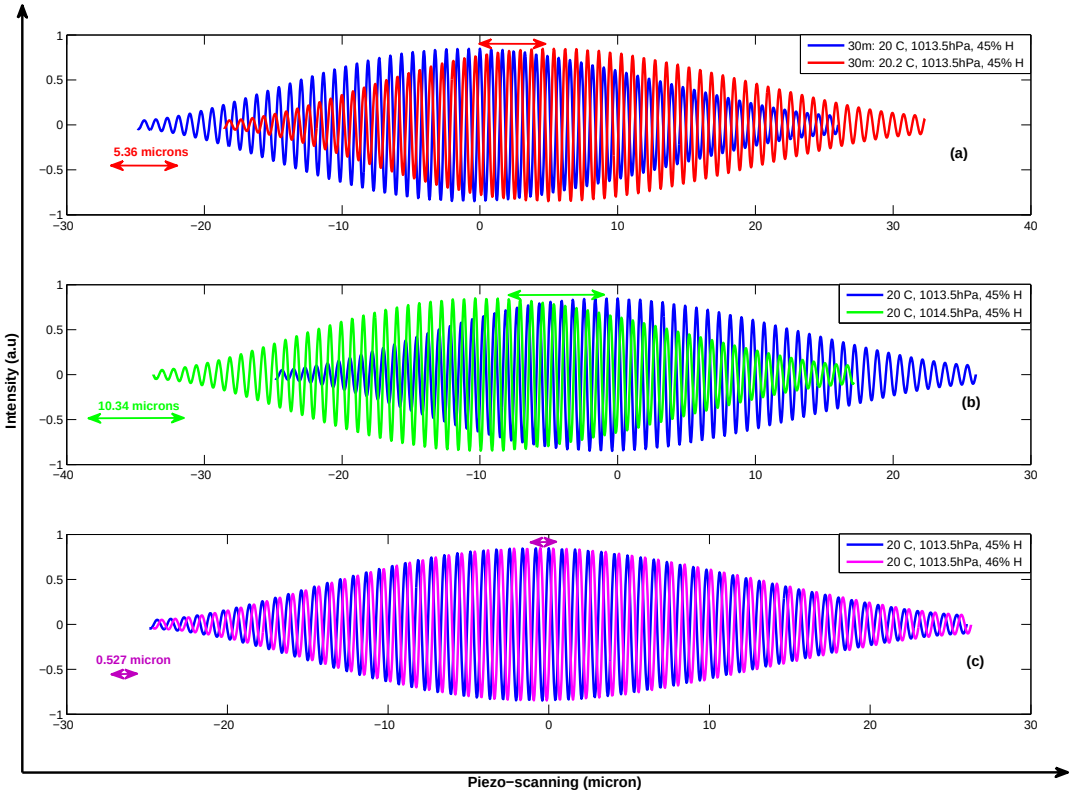

FIG. 9. The effect of variation in the environmental parameters (a) temperature, (b) pressure and (c) humidity on the cross-correlation pattern.

III. CONTINUOUS MODEL FOR CROSS-CORRELATION FUNCTIONS

In this section we study fringe positioning and asymptotic convergence of correlation patterns for large delay distances. The cross-correlation is a sum of all harmonics of a slowly varying function, PSD, multiplied by an oscillating phase factor. We would now like to extend the discrete model to a continuous one by using an integral in the formulation of the cross-correlation function $\Gamma(X)$, instead of a series in Eq. (25). Clearly the PSD, $|a_m|^2$, in Eq. (25) varies slowly with m; however the cosine function does not, and therefore it is not valid to directly replace the sum by an integral. Instead, the corresponding integral must be found via other methods. In this section we use the Poisson summation formula to write a series of all possible cross-correlation functions for the chosen PSD and dispersive media. From this series we obtain the integral formulation of the cross-correlation function for a specific delay distance.

We would like to note here that the transition from a discrete to a continuous model can be expressed using simpler methods. This is only true if the mode-locked laser is operating at a repetition frequency lower than few tens of megahertz where the contribution of the offset frequency is insignificant. Recent developments in femtosecond laser technology allow for faster repetition frequencies with fewer modes [31]. There are also examples of experiments where the frequency comb has been filtered with a Fabry-Perot cavity [20]. In addition, in the limit of large delay distances the precise values of the offset and repetition frequencies become important since particular frequencies contribute to the formation of specific fringes in the cross-correlation [28]. In these cases it would be invalid to neglect the offset frequency. Therefore, we have developed a general rigorous formula of the cross-correlation function applied to any type of train of pulses emitted from a frequency comb laser. This was made possible by using the Poisson summation formula.

Let us extend the definition of the discrete coefficients a_m from Eq. (8) to continuous variables, where

$$\mathcal{E}^p(0,t) = \sum_{m=0}^{\infty} a_m \exp(im\omega_r t) \tag{30}$$

To be able to map a continuous spectrum to the discrete one we need to define the electric field from Eq. (30) having a finite support $[-T_r/2, T_r/2]$ as

$$\mathcal{E}^p_{T_r}(0,t) = \mathcal{E}^p(0,t)\chi_{\left[-\frac{T_r}{2},\frac{T_r}{2}\right]}(t) \tag{31}$$

where the χ function is defined similarly to Eq. (17) with a time distance equal to T_r, the inter-pulse time interval. The Fourier transform of $\mathcal{E}^p_{T_r}(0,.)$ is given by

$$\begin{aligned}\mathcal{F}\left[\mathcal{E}^p_{T_r}(0,.)\right](\omega) &= \frac{1}{2\pi}\mathcal{F}\left[\chi_{T_r}(.)\right](\omega) * \mathcal{F}\left[\mathcal{E}^p(0,.)\right](\omega) \\ &= \sum_{m=0}^{\infty} a_m \,\mathrm{sinc}\left[(\omega - m\omega_r)\frac{T_r}{2}\right]\end{aligned} \tag{32}$$

In particular,

$$\mathcal{F}\left[\mathcal{E}^p_{T_r}(0,.)\right](m\omega_r) = a_m \;\text{ for } m = 0,1,2... \tag{33}$$

We define for real ω, $-\infty < \omega < \infty$, the power spectral density as

$$S(\omega + \omega_0) = |\mathcal{F}\left[\mathcal{E}^p_{T_r}(0,.)\right](\omega)|^2. \tag{34}$$

Then

$$S(m\omega_r + \omega_0) = |a_m|^2 \;,\; m = 0,1,..., \tag{35}$$

By substituting Eq. (35) into Eq. (25) we have

$$\Gamma(X) = \sum_{m=0}^{\infty} S(m\omega_r + \omega_0) \cos\left[(m\omega_r + \omega_0) n(m\omega_r + \omega_0) \frac{X}{c}\right] \tag{36}$$

Let $\bar{n}$ be the mean refractive index, write $\cos(x) = \frac{1}{2}\exp(ix) + \frac{1}{2}\exp(-ix)$ in Eq. 36, and substract and add $\bar{n}$ from $n(m\omega_r + \omega_0)$ in the exponentials to obtain

$$\begin{aligned}\Gamma(X) = \frac{1}{2}\sum_{m=0}^{\infty} & S(m\omega_r + \omega_0) \exp\left\{i(m\omega_r + \omega_0)\left[n(m\omega_r + \omega_0) - \bar{n}\right]\frac{X}{c}\right\} \exp\left[i\omega_0 \frac{X}{c}\bar{n}\right] \\ & \times \exp\left[im\omega_r \frac{X}{c}\bar{n}\right] \\ & + \frac{1}{2}\sum_{m=0}^{\infty} S(m\omega_r + \omega_0) \exp\left\{-i(m\omega_r + \omega_0)\left[n(m\omega_r + \omega_0) - \bar{n}\right]\frac{X}{c}\right\} \exp\left[-i\omega_0 \frac{X}{c}\bar{n}\right] \\ & \times \exp\left[-im\omega_r \frac{X}{c}\bar{n}\right]\end{aligned} \tag{37}$$

We define:

$$\mathcal{H}_X(\omega) = \begin{cases} S(\omega + \omega_0) \exp\left\{i(\omega + \omega_0)\left[n(\omega + \omega_0) - \bar{n}\right]\frac{X}{c}\right\} \exp\left[i\omega_0 \bar{n}\frac{X}{c}\right], & \omega \geq 0 \\ S(-\omega + \omega_0) \exp\left\{i(\omega - \omega_0)\left[n(-\omega + \omega_0) - \bar{n}\right]\frac{X}{c}\right\} \exp\left[-i\omega_0 \bar{n}\frac{X}{c}\right], & \omega \leq 0 \end{cases} \tag{38}$$

and

$$\mathcal{H}_X(0) = S(\omega_0) \cos\left[\omega_0 n(\omega_0)\frac{X}{c}\right] \tag{39}$$

Then

$$\Gamma(X) = \mathcal{H}_X(0) + \frac{1}{2}\sum_{m=1}^{\infty} \mathcal{H}_X(m\omega_r) \exp\left[im\omega_r \frac{X}{c}\bar{n}\right] + \frac{1}{2}\sum_{m=1}^{\infty} \mathcal{H}_X(-m\omega_r) \exp\left[-im\omega_r \frac{X}{c}\bar{n}\right] \tag{40}$$

Now $|S(\omega_0)|$ is negligibly small, and so we may replace $\mathcal{H}_X(0)$ in Eq. (40) by $\frac{1}{2}\mathcal{H}_X(0)$. Thus, with a negligibly small error,

$$\Gamma(X) = \frac{1}{2}\sum_{m=-\infty}^{\infty} \mathcal{H}_{\mathcal{X}}(m\omega_r) \exp\left[im\omega_r \frac{X}{c}\bar{n}\right] \tag{41}$$

This form is convenient for the application of the Poisson summation formula. Thus with

$$h_X(t) = \frac{1}{2\pi}\int_{-\infty}^{\infty} \mathcal{H}_X(\omega) \exp(i\omega t) d\omega \tag{42}$$

the inverse Fourier transform of $\mathcal{H}_X$, it holds that

$$\begin{aligned}\Gamma(X) &= \frac{1}{2}\sum_{m=-\infty}^{\infty}\mathcal{F}\left[h_X(.)\right](m\omega_r)\exp\left[im\omega_r\frac{X}{c}\bar{n}\right] \\ &= \frac{1}{2}\sum_{m=-\infty}^{\infty}\mathcal{F}\left[h_X(.+\frac{X}{c}\bar{n})\right](m\omega_r) \\ &= \frac{1}{2}T_r\sum_{\ell=-\infty}^{\infty}h_X\left(\ell T_r+\frac{X}{c}\bar{n}\right)\end{aligned} \tag{43}$$

Here the Poisson summation formula

$$\sum_{m=-\infty}^{\infty}\left[\mathcal{F}h_X\right](m\omega_r) = \frac{2\pi}{\omega_r}\sum_{\ell=-\infty}^{\infty}h_X\left(\frac{2\pi}{\omega_r}\ell\right) \tag{44}$$

with $\omega_r = \frac{2\pi}{T_r}$ has been used. This series expression for $\Gamma(X)$ in Eq. (43) reduces to at most a single term when h_X has support length $\leq T_r$.

The pulse propagating in the long arm undergoes substantial broadening in the dispersive media. This in turn broadens the cross-correlation function. In the above analysis we are in the regime where the extent of the cross-correlation function is still smaller than the laser cavity length, in other words the intensity observed by the detector at the upper and lower bounds of the finite support, $[-T_r/2, T_r/2]$, is negligible. We can demonstrate that the series in Eq. (43) contains at most one dominant term (ℓ). This is explicitly derived in Reference [28]. From a physical point of view, the integer ℓ denotes the multiple of the laser cavity length at a given delay distance X and ℓT_r is the propagation time of a pulse in "vacuum". In the case where $X > 0$ the integer ℓ must be negative. We would like to define the time variable (t) as

$$t \equiv \bar{n}\frac{X}{c} \pmod{T_r}. \tag{45}$$

Using this, for a given ℓ, Eq.(43) can be written as

$$\Gamma(X) = \frac{T_r}{2}h_X(t) \tag{46}$$

Expressing $h_X(t)$ in terms of the PSD, we get

$$\begin{aligned}h_X(t) = &\frac{1}{2\pi}\int_{-\infty}^{0}S(\omega+\omega_0)\exp\left\{i(\omega-\omega_0)\left[n(-\omega+\omega_0)-\bar{n}\right]\frac{X}{c}\right\}\exp\left[-i\omega_0\bar{n}\frac{X}{c}\right]\exp(i\omega t)d\omega \\ &+\frac{1}{2\pi}\int_{0}^{\infty}S(\omega+\omega_0)\exp\left\{i(\omega+\omega_0)\left[n(\omega+\omega_0)-\bar{n}\right]\frac{X}{c}\right\}\exp\left[i\omega_0\bar{n}\frac{X}{c}\right]\exp(i\omega t)d\omega\end{aligned} \tag{47}$$

Changing $-\omega$ into $\omega \in [0, \infty]$ in the first integral and adding the two integrals yields

$$h_X(t) = \frac{1}{\pi} \int_0^\infty S(\omega + \omega_0) \cos \left\{ (\omega + \omega_0) \left[n(\omega + \omega_0) - \bar{n} \right] \frac{X}{c} + \omega_0 \bar{n} \frac{X}{c} + \omega t \right\} d\omega \tag{48}$$

Equation (48) states that for any arbitrary delay distance X a cross-correlation pattern $h_X(t)$ can be obtained by varying the time delay (t) where $-T_r/2 \leq t \leq T_r/2$. In practice, this time (t) can be obtained by setting up a scanning short arm which has a total length of the laser cavity.

IV. POSITION OF THE BRIGHTEST FRINGE AFTER PROPAGATION IN NONLINEAR DISPERSIVE MEDIA

The shift of the brightest fringe due to the dispersion will be discussed where the medium is limited to its quadratic approximation. This quadratic approximation has the mathematical advantage that the Fresnel transform can be used. Also it has been shown that optimal results can be obtained with the quadratic or the cubic dispersion approximation and including higher order terms does not improve the accuracy [25]. The following analysis will be based on the method introduced by Jones [29] for an electromagnetic pulse in dispersive media.

We aim to derive an expression for the cross-correlation using the properties of the autocorrelation. Our analysis starts from Eq. (48) where we set $X = 0$. This is the case of an interferometer at equal arms, i.e an autocorrelator. In this case, we obtain

$$h_{X=0}(t) = \frac{1}{\pi} \int_0^\infty S(\omega + \omega_0) \cos(\omega t) d\omega \tag{49}$$

For convenience we will separate the time variable of the autocorrelation and the cross-correlation. Let τ_c be the full duration of the initial autocorrelation where $\tau_c < T_r$. We assume that the function $h_{X=0}(t_0)$ is real and even (Eq. (49)), and vanishes outside an interval $[-\frac{1}{2}\tau_c, \frac{1}{2}\tau_c]$ where $\tau_c < T_r$. The Wiener-Khintchin theorem states that the autocorrelation and the power spectral density are a Fourier transform pair, hence for $\omega > 0$

$$\begin{aligned} S(\omega + \omega_0) &= \int_{-\infty}^\infty h_{X=0}(t_0) \exp\left(-i\omega t_0\right) dt_0 \\ &= \int_{-\infty}^\infty h_{X=0}(t_0) \cos(\omega t_0) dt_0 \end{aligned} \tag{50}$$

By using Eq. (50) in Eq. (48) and interchanging integrals, we obtain

$$h_X(t) = \frac{1}{\pi}\int_{-\infty}^{\infty} h_{X=0}(t_0)dt_0 \int_0^{\infty} \cos\left[k(\omega+\omega_0)X - \omega\bar{n}\frac{X}{c} + \omega t\right]\cos(\omega t_0)d\omega \qquad (51)$$

where $k(\omega+\omega_0) = n(\omega+\omega_0)(\omega+\omega_0)/c$. We use the fact the the medium has a quadratic dispersion relation described in terms of Taylor expansion that is twice differentiable in the neighborhood of the maximum frequency of the spectrum ω_c also known as the carrier frequency. This allows us to write $k(\omega+\omega_0) = \alpha\omega^2 + \beta\omega + \gamma$. We now consider the case of large delay distance X. To be precise, we assume that X is so large that for all t_0 in the support $[-\tau_c/2, -\tau_c/2]$ of $h_{X=0}(t_0)$, we have

$$\frac{t_0}{2\sqrt{\alpha X}} << 1 \qquad (52)$$

Using this we can derive an expression for $h_X(t)$ in a simple integral form as

$$h_X(t) = \frac{R}{2\pi}\sqrt{\frac{\pi}{2\alpha X}}\cos\left[\gamma X - \frac{\left(\beta X - \bar{n}\frac{X}{c} + t\right)^2}{4\alpha X} + \theta\right]\int_{-\infty}^{\infty} dt_0 h_{X=0}(t_0)]\cos\left[\frac{\beta X - \bar{n}\frac{X}{c} + t}{2\alpha X}t_0\right] \qquad (53)$$

The details of this calculation are given in Appendix A. In the above equation R and θ are parameters dependent on the dispersion properties of the medium and are also explained in Appendix A. Details regarding the cross-correlation from Eq. (53) at large delays are discussed in [28]. For the moment, we just say that the time scale $\sqrt{4\alpha X}$ plays a role in the distortion of the cross-correlation. Therefore, we can define a dimensionless function "$\zeta(X)$" as

$$\zeta(X) = \frac{\tau_c}{\sqrt{(4\alpha X)}} = \frac{\tau_c}{\sqrt{\frac{2}{c}\left[2\frac{dn(\omega)}{d\omega} + \omega\frac{d^2n(\omega)}{d\omega^2}\right]_{\omega=\omega_0} X}} \qquad (54)$$

The constant τ_c can be simply obtained either from the Fourier transform of the PSD or from experimental measurements using an autocorrelator. The function $\zeta(X)$ is plotted for various delay distances in Fig. 10.

In order to study the variation of the position of the brightest fringe in dispersive media we have simulated a series of cross-correlation patterns from 0 to 100 m delay in air with steps of one cavity length ($\sim$ 30 cm). For each pattern, the position where the maximum fringe visibility is obtained has been registered. We refer to this position as d_{mc}. At the same time consider the distance d_{n_g} defined by

$$d_{n_g} = \frac{ql_{pp}}{n_g}. \qquad (55)$$

In the experiment accurate knowledge of the pulse-to-pulse distance l_{pp} is available since the repetition frequency f_r of the laser is locked. q is an integer number and n_g is the group refractive index at the peak of the frequency spectrum of the carrier frequency. We would like to emphasize again that the position where the maximum coherence in the fringe pattern occurs differ from the position d_{n_g} (at the carrier frequency). The discrepancy between d_{mc} and d_{n_g} is due to the chirp acquired by the pulse, which has an asymmetric spectrum, in the long arm of the interferometer. The difference ($dchirp = d_{n_g} - d_{mc}$)is plotted as a function of the propagation distance in air in Fig. 10. *dchirp* is small compared to the delay distance (meters), but it has a substantial impact for the evaluation of the delay distance. Simulations

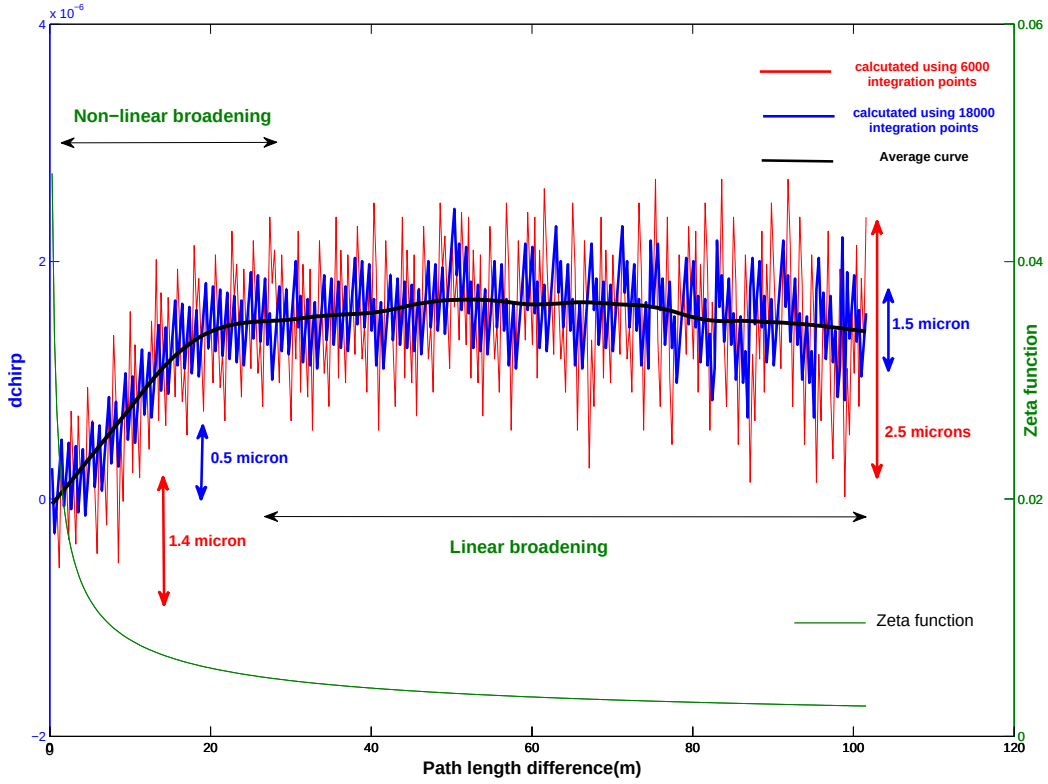

FIG. 10. Shift of the position of the fringe having maximum visibility as a function of the path length difference. The zeta function is also plotted, showing the non-linear dispersion depth.

have been performed under one fixed environmental condition (20 C, 1013hPa, 45%H). For the numerical integration, a standard resolution of 6000 integration points (corresponding to a 12 nm step size) and a high resolution of 18000 integration points (corresponding to

a 4 nm step size) have been used. This was done to show that the numerical integration shows statistical errors when a high precision is required. These statistical variations can be averaged-out. Curves using a standard resolution(red), a high resolution(blue), and the average curve are shown in Fig. 10. It can be clearly seen that d_{n_g} and d_{mc} are different at different length scales. The shift of the position of the fringe at maximum coherence of the correlation pattern varies non-linearly when the delay distance is approximately less than 30 m. After 30 m, this shift stabilizes but always differs from d_{n_g}.

We recall again the $\zeta(X)$ function from Eq. (54). The variable X in the $\zeta(X)$ function denotes the delay distance in the interferometer. We assumed that the reference arm placed in air is short (30 cm), and dispersion in this arm can be neglected. In the long arm, the pulse propagates for several tens of meters. The parameter ζ is plotted in Fig. 10 as a function of the propagation distance from 0 up to 100m. The dispersive term in ζ is calculated from the equation for refractive index, the Edlén's equation, used previously to derive the distances under the same environmental conditions. It is clearly seen in Fig.10 when the propapagation distance increases, ζ tends asymptotically to zero. The asymptotic linear behaviour of ζ starts to dominate the initial non-linear behaviour after approximately 30 m in air. This property of the function ζ and the resulting correction *dchirp* is dependent on the shape of the PSD of the laser source. If air is the dispersive medium, a variation in the environmental parameters will give rise to a different ζ function and hence the curve for the correction *dchirp* will be different.

V. NON-LINEAR DISPERSION DEPTH IN DISPERSIVE MEDIA

With the numerical analysis in the previous section we were able to identify the delay distance in air where non-linear dispersion effects cease acting on the cross-correlation shape and position. Using this method it is possible to indicate the depth of non-linearity in any optical medium. We did this by choosing a particular point on the $\zeta(X)$ function curve, namely $P(X_p, Y_p)$ where P is the nearest point to the origin $O(0, 0)$. The distance between the origin and a point $(X, Y = \zeta(X))$ is defined by

$$r = \sqrt{X^2 + \zeta(X)^2} \tag{56}$$

The point P is located where the smallest value of r occurs. Hence, with $r = r(X)$, the X_p coordinate is the solution of the equation

$$\frac{d}{dX} r(X) = 0 \tag{57}$$

Once X_p is obtained, we calculate Y_p as $Y_p = \zeta(X_p)$. The tangent line $y(X)$ at the point $P(X_p, Y_p)$ is given by

$$y(X) = \zeta^{'}(X_p)X + y_0 \tag{58}$$

where $\zeta^{'}(X_p)$ is the derivative of $\zeta(X)$ at $X = X_p$. Knowing $\zeta^{'}(X_p)$ and $P(X_p, Y_p)$, the intersection point y_0 of the tangent line at (X_p, Y_p) and the y-axis can be easily determined.

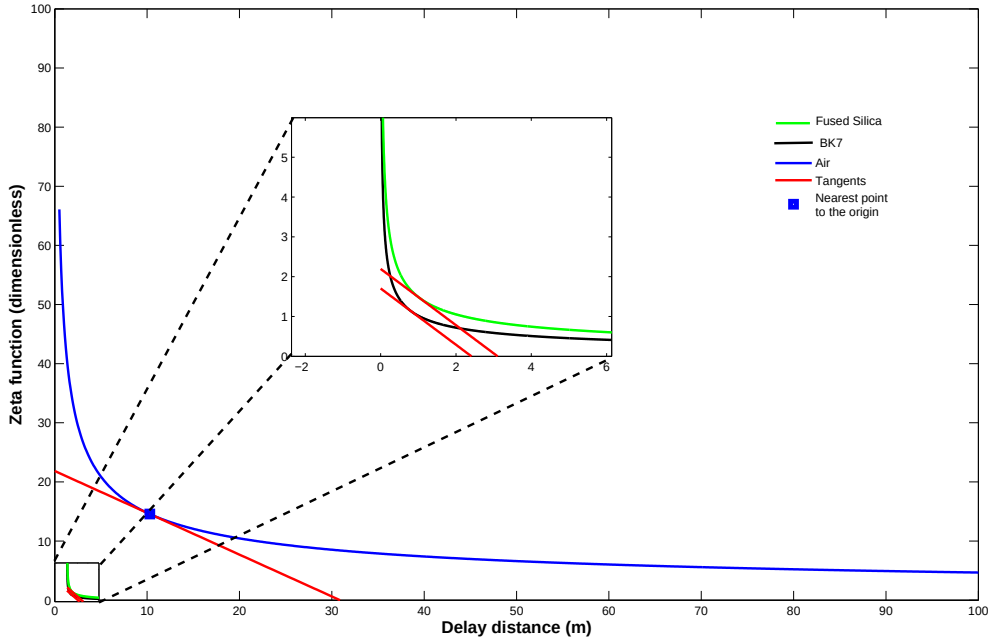

FIG. 11. Zeta function showing the non-linear dispersion depths in various transparent media.

In Fig. 11 we plot the ζ function in various media. The tangent lines at the particular points P have also been drawn. We define the distance where non-linear dispersion is no longer significant as the Non-linear Dispersion Depth (NDD). This is the distance after which non-linear effects do not play a dominant role in the cross-correlation function and

linear broadening takes over. This distance NDD is obtained as the intersection point of the tangent line in Eq. (58) with the X-axis. By setting $y = 0$, we obtain

$$\text{NDD} = -\frac{y_0}{\zeta'(X_p)} = \frac{3}{2}\sqrt[3]{\frac{\tau_c^2}{\alpha}} \tag{59}$$

Equation (59) shows the effective distance of non-linear dispersion effects on cross-correlations obtained from a light source having a coherence time τ_c and a carrier frequency ω_c propagating in a refractive medium with a group delay dispersion α at ω_c. For standard air NDD=30 m. Similar calculations and simulations (Fig. 11) are carried-out for the $BK7$ and fused silica glasses. The refractive index equations of these materials have been taken from the Sellmeier equation. We obtained NDD_{BK7}=2.4 m and NDD_{silica}= 3 m. The accuracy of the calculated distance or thickness depends on the precision of the refractive index equation. At best, 5 significant digits are available for Sellmeier 's equation, whereas, in the case of the Edlén's equation for air, up to 9 significant digits are accurately known. This can be useful for systems using fiber based delay lines.

VI. CONCLUSION

We have analysed cross-correlation functions formed after pulse propagation in dispersive media in an unbalanced Michelson interferometer. Discrete models of cross-correlation patterns generated from the discrete spectrum of the optical frequency comb have been compared to experimental measurements of pulse propagation in 200m of air. We observe that the shape of the power spectral density plays a large role in determining the final shape of the correlation pattern. Correlation patterns formed by pulses with symmetric spectra, after propagation in a dispersive media tend to be linearly stretched, leading to an easy retrieval of the position of the brightest fringe, by use of the group refractive index of the medium. In contrast, correlation patterns formed by pulses having non symmetric spectra show a shift of the position of the brightest fringe when compared to the position derived from the group refractive index. This shift varies non-linearly with the delay distance and stabilizes after reaching a certain delay. This shift can be predicted using the continuous model for cross-correlation patterns. Using the integral-based continuous cross-correlation function we have shown that the shift of the central brightest fringe varies non-linearly with the delay distance and stabilizes after reaching a certain delay. The delay distance where

non-linearity plays an important role can be scaled for every dispersive media.

VII. ACKNOWLEDGEMENTS

The authors would like to thank Omar El Gawhary for extensive discussions. The authors gratefully acknowledge J. J. M. Braat for his thoughtful comments on the manuscript. This work is part of the Industrial Partnership Programme (IPP) Metrology with Frequency Comb Laser (MFCL) of the Stichting voor Fundamenteel Onderzoek der Materie (FOM), which is supported financially by Nederlandse Organisatie voor Wetenschappelijk Onderzoek (NWO). The IPP MFCL is co-financed by VSL, TNO and ASML. The research within this work is also a part of EURAMET joint research project and has received funding from the European Community's Seventh Framework Programme, ERA-NET Plus, under Grant Agreement No. 217257.

APPENDIX A

We begin with the integral representation of the cross-correlation function

$$h_X(t) = \frac{1}{\pi}\int_{-\infty}^{\infty} h_{X=0}(t_0)dt_0 \int_0^{\infty} \cos\left[k(\omega+\omega_0)X - \omega\bar{n}\frac{X}{c} + \omega t\right]\cos(\omega t_0)d\omega \tag{A.60}$$

where,

$$\begin{aligned} k(\omega+\omega_0) &= n(\omega+\omega_0)(\omega+\omega_0)/c \\ &= k(\omega_c+\omega_0) + k^{'}(\omega_c+\omega_0)(\omega-\omega_c) + \frac{1}{2}k^{''}(\omega_c+\omega_0)(\omega-\omega_c)^2 \\ &= \alpha\omega^2 + \beta\omega + \gamma \end{aligned} \tag{A.61}$$

By using Eq. (A.61) in Eq. (A.60) we obtain

$$h_X(t) = \frac{1}{\pi}\int_{-\infty}^{\infty} h_{X=0}(t_0)dt_0 \int_0^{\infty} \cos\left[(\alpha\omega^2+\beta\omega+\gamma)X - \omega\bar{n}\frac{X}{c} + \omega t\right]\cos(\omega t_0)d\omega \tag{A.62}$$

By converting the product of cosines into a sum of cosines and by completing the square in the cosines of Eq. (A.62), we get

$$h_X(t) = \frac{1}{2\pi}\int_{-\infty}^{\infty} h_{X=0}(t_0)dt_0 \int_0^{\infty} \left\{ \cos\left[\left(\sqrt{\alpha X}\omega - \frac{\left(\beta X - \bar{n}\frac{X}{c} + t + t_0\right)}{2\sqrt{\alpha X}} \right)^2 + \gamma X - \frac{\left(\beta X - \bar{n}\frac{X}{c} + t + t_0\right)^2}{4\alpha} \right] + \cos\left[\left(\sqrt{\alpha X}\omega - \frac{\left(\beta X - \bar{n}\frac{X}{c} + t - t_0\right)}{2\sqrt{\alpha X}} \right)^2 + \gamma X - \frac{\left(\beta X - \bar{n}\frac{X}{c} + t - t_0\right)^2}{4\alpha X} \right] \right\} d\omega \tag{A.63}$$

Next the following change of variables

$$\begin{aligned} \Omega_{\pm} &= \sqrt{\alpha X}\omega - \frac{\left(\beta X - \bar{n}\frac{X}{c} + t \pm t_0\right)}{2\sqrt{\alpha X}} \\ d\Omega_{\pm} &= \sqrt{\alpha X}d\omega \\ \rho_{\pm} &= \gamma X - \frac{\left(\beta X - \bar{n}\frac{X}{c} + t \pm t_0\right)^2}{4\alpha X} \\ f_X(t \pm t_0) &= -\frac{\left(\beta X - \bar{n}\frac{X}{c} + t \pm t_0\right)}{2\sqrt{\alpha X}} \end{aligned} \tag{A.64}$$

is applied. Then Eq. (A.62)

$$\begin{aligned} h_X(t) &= \frac{1}{2\pi}\int_{-\infty}^{\infty} h_{X=0}(t_0)dt_0 \int_{f_X(t\pm t_0)}^{\infty} \left[\cos\left(\Omega_+^2 + \rho_+\right)d\Omega + \cos\left(\Omega_-^2 + \rho_-\right)d\Omega\right] \\ &= \frac{1}{4\pi}\sqrt{\frac{\pi}{2\alpha X}}\int_{-\infty}^{\infty} dt_0 h_{X=0}(t_0)\left\{\cos(\rho_+) - 2\cos(\rho_+)\mathcal{C}\left(\sqrt{\frac{2}{\pi}}f_X(t+t_0)\right)\right. \\ &\quad - \left[\sin(\rho_+) - 2\sin(\rho_+)\mathcal{S}\left(\sqrt{\frac{2}{\pi}}f_X(t+t_0)\right)\right] + \cos(\rho_-) - 2\cos(\rho_-)\mathcal{C}\left(\sqrt{\frac{2}{\pi}}f_X(t-t_0)\right) \\ &\quad \left. - \left[\sin(\rho_-) - 2\sin(\rho_-)\mathcal{S}\left(\sqrt{\frac{2}{\pi}}f_X(t-t_0)\right)\right]\right\} \end{aligned} \tag{A.65}$$

where the functions $\mathcal{C}$ and $\mathcal{S}$ are the Fresnel integrals and defined as

$$\begin{aligned} \mathcal{C}(z) &= \int_0^z \cos\left(\frac{\pi}{2}\xi^2\right)d\xi \\ \mathcal{S}(z) &= \int_0^z \sin\left(\frac{\pi}{2}\xi^2\right)d\xi \end{aligned} \tag{A.66}$$

We now consider the case of large delay distance X. To be precise, we assume that X is so large that for all t_0 in the support $[-\tau_c/2, -\tau_c/2]$ of $h_{X=0}(t_0)$, we have

$$\frac{|t_0|}{2\sqrt{\alpha X}} << 1 \tag{A.67}$$

In this approximation, we rewrite $\rho_\pm$ and $f_X(t \pm t_0)$ as

$$\rho_\pm = \gamma X - \frac{\left(\beta X - \bar{n}\frac{X}{c} + t\right)^2}{4\alpha X} \mp \frac{\left(\beta X - \bar{n}\frac{X}{c} + t\right)}{2\alpha X} t_0$$
$$f_X(t) = f_X(t \pm t_0) = -\frac{\left(\beta X - \bar{n}\frac{X}{c} + t\right)}{2\sqrt{\alpha X}} \tag{A.68}$$

Using the $\rho_\pm$ from Eq. (A.68) above and expanding the cosines and sines in Eq. (A.65) as a trigonometric sum we observe that the integral

$$\int_{-\infty}^{\infty} dt_0 h_{X=0}(t_0) \sin\left(\frac{\left(\beta X - \bar{n}\frac{X}{c} + t\right)}{2\alpha X} t_0\right) = 0 \tag{A.69}$$

because $h_{X=0}(t_0)$ is an even function. Therefore, the only contributing terms arise from

$$\rho = \gamma X - \frac{\left(\beta X - \bar{n}\frac{X}{c} + t\right)^2}{4\alpha X} + \frac{\left(\beta X - \bar{n}\frac{X}{c} + t\right)}{2\alpha X} t_0 \tag{A.70}$$

Equation. (A.65) can be written as

$$h_X(t) = \frac{1}{2\pi}\sqrt{\frac{\pi}{2\alpha X}} \int_{-\infty}^{\infty} dt_0 h_{X=0}(t_0) \left\{ \left[1 - 2\mathcal{C}\left(\sqrt{\frac{2}{\pi}} f_X(t)\right)\right] \cos(\rho) \right.$$
$$\left. - \left[1 - 2\mathcal{S}\left(\sqrt{\frac{2}{\pi}} f_X(t)\right)\right] \sin(\rho) \right\} \tag{A.71}$$

When a, b are real, we can write $a\cos x - b\sin x = R\cos(x+\theta)$. In our case R and θ are given by

$$R = \sqrt{a^2 + b^2} = \sqrt{\left[1 - 2\mathcal{C}\left(\sqrt{\frac{2}{\pi}} f_X(t)\right)\right]^2 + \left[1 - 2\mathcal{S}\left(\sqrt{\frac{2}{\pi}} f_X(t)\right)\right]^2}$$
$$\tan\theta = \frac{b}{a} = \frac{1 - 2\mathcal{S}\left(\sqrt{\frac{2}{\pi}} f_X(t)\right)}{1 - 2\mathcal{C}\left(\sqrt{\frac{2}{\pi}} f_X(t)\right)} \tag{A.72}$$

Using (A.72) in Eq. (A.71), we obtain

$$h_X(t) = \frac{R}{2\pi}\sqrt{\frac{\pi}{2\alpha X}} \int_{-\infty}^{\infty} dt_0 h_{X=0}(t_0) \cos\left[\gamma X - \frac{\left(\beta X - \bar{n}\frac{X}{c} + t\right)^2}{4\alpha X} + \frac{\left(\beta X - \bar{n}\frac{X}{c} + t\right)}{2\alpha X} t_0 + \theta\right] \tag{A.73}$$

We again expand the cosine as a trigonometric sum and using Eq. (A.69) we can write $h_X(t)$ in a simple integral form as

$$h_X(t) = \frac{R}{2\pi}\sqrt{\frac{\pi}{2\alpha X}} \cos\left[\gamma X - \frac{\left(\beta X - \bar{n}\frac{X}{c} + t\right)^2}{4\alpha X} + \theta\right] \int_{-\infty}^{\infty} dt_0 h_{X=0}(t_0)] \cos\left[\frac{\beta X - \bar{n}\frac{X}{c} + t}{2\alpha X} t_0\right] \tag{A.74}$$

[1] D. J. Jones, S. A. Diddams, J. K. Ranka, A. Stentz, R. S. Windeler, J. L. Hall, S. T. Cundiff, Science **288** 635 (2000).

[2] R. Holzwarth, Th. Udem, T.W. Hänsch, J. C. Knight, W. J. Wadsworth, and P. St. J. Russell, Phys. Rev. Lett **85**, 2264 (2000).

[3] S. T. Cundiff and J. Ye, Rev. Mod. Phys. **75**, 325 (2003).

[4] S. A. Diddams, J. C. Bergquist, S. R. Jefferts, C. W. Oates, Science **306**, 1318 (2004).

[5] Th.Udem, R.Holzwarth, and T.W.Hänsch, Nature **416**, 233 (2002).

[6] L. Hollberg, C. W. Oates, E. A. Curtis, E. N. Ivanov, S. A. Diddams, T. Udem, H. G. Robinson, J. C. Bergquist, R. J. Rafac, W. M. Itano, R. E. Drullinger, and D. J. Wineland, IEEE J. Quant. Elect. **37**, 1502 (2001).

[7] J. Ye, H. Schnatz, and L. W. Hollberg, IEEE J. Select. Top. Quant. Elect. **9**, 1041 (2003).

[8] B. Lamine, C. Fabre and N. Treps, Phys. Rev. Lett. **101**, 123601 (2008).

[9] N. C. Menicucci, S. T. Flammia and O. Pfister. Phys. Rev. Lett. **101**, 130501 (2008).

[10] S. Schiller, Opt. Lett. **27**, 766 (2002).

[11] M. J. Thorpe and J. Ye, Appl. Phys. B **91**, 397 (2008).

[12] J. Mandon, G. Guelachvili and N. Picqué, Nature Photonics **3**, 99 (2009).

[13] R. Paschotta, A. Schlatter, S. C. Zeller, H. R. Telle, U. Keller, Appl. Phys. B **79**, 163 (2004).

[14] R. K. Shelton, S. M. Foreman, L. S. Ma, J. L. Hall, H. C. Kapteyn, M. M. Murnane, M. Notcutt, and J. Ye, Opt. Lett. **27**, 312 (2002).

[15] T. M. Fortier, D. J. Jones, J. Ye, and S. T. Cundiff, R. S. Windeler, Opt. Lett. **27**,1436 (2002).

[16] J.Ye, Opt. Lett. **29**, 1153 (2004).

[17] J. J. M. Braat (unpublished); S. N. Bagayev (unpublished)

[18] M. Cui, R. N. Schouten, N. Bhattacharya and S. A. van den Berg, J.E.O.S. - Rapid Publications **3** 08003 (2008)

[19] Y. Salvade, N. Schuhler, S. Leveque and S. Le Floch, Appl. Opt. **47**, 2715 (2008) and references therein.

[20] K.N.Joo, Y.Kim and S.W.Kim, "Distance measurements by combined method based on a femtosecond pulse laser", Opt. Exp. **16**, 19799 (2008) and references therein.

[21] P. Balling, P. Křen, P. Mašika, S. A. van den Berg, Opt. Exp. **17**, 9300-9313 (2009).

[22] M. Cui, M. G. Zeitouny, N. Bhattacharya, S. A. van den Berg, H. P. Urbach, and J. J. M. Braat, Opt. Lett. **34**, 1982-1984 (2009).

[23] I. Coddington, W. C. Swann, L. Nenadovic and N. R. Newbury, Nature Photonics **3**, 351-356 (2009).

[24] L. Wang, H. X. Zhang and R. P. Wang, JETP Letters **84**, 425 (2006).

[25] K. E. Oughstun and N. A. Cartwright, J. Mod. Opt. **52**, 1089 (2005) and references therein.

[26] S. P. Dijaili, A. Dienes and J. S. Smith, IEEE J. Quant. Elect. **26**, 1158 (1990).

[27] A. M. Nugrowati, S. F. Pereira, and A. S. van de Nes, Phys. Rev. A **77**, 053810 (2008).

[28] M. G. Zeitouny, M. Cui, N. Bhattacharya, S.A. van den Berg, A. J. E. M. Janssen, and H.P. Urbach, submitted simultaneously to Phys. Rev. A

[29] J. Jones, Am. J. Phys. **42**, 43 (1974).

[30] K.P.Birch and M.J.Downs, Metrologia **31**, 315 (1994).

[31] A. Bartels, D. Heinecke, and S. A. Diddams, Opt. Lett. **33**, 1905-1907 (2008)